

Monitoring Ion Channel Function In Real Time Through Quantum Decoherence

L.T. Hall,¹ C.D. Hill,¹ J.H. Cole,^{1,2} B. Städler,³ F. Caruso,³ P. Mulvaney,⁴ J. Wrachtrup,⁵ and L.C.L. Hollenberg¹

¹Center for Quantum Computer Technology, School of Physics, University of Melbourne, VIC 3010, Australia

²Institute für Theoretische Festkörperphysik and DFG-Center for Functional Nanostructures (CFN),
Universität Karlsruhe, 76128 Karlsruhe, Germany

³Centre for Nanoscience and Nanotechnology, Department of Chemical and Biomolecular Engineering,
The University of Melbourne, Parkville, Victoria 3010, Australia

⁴School of Chemistry and Bio21 Institute, University of Melbourne, Parkville, Victoria 3010, Australia

⁵Physikalisches Institut, Universität Stuttgart, 70550 Stuttgart, Germany

In drug discovery research there is a clear and urgent need for non-invasive detection of cell membrane ion channel operation with wide-field capability [1]. Existing techniques are generally invasive [2], require specialized nano structures [3, 4, 5, 6], or are only applicable to certain ion channel species [7]. We show that quantum nanotechnology has enormous potential to provide a novel solution to this problem. The nitrogen-vacancy (NV) centre in nano-diamond is currently of great interest as a novel single atom quantum probe for nanoscale processes [8, 9, 10, 11, 12, 13, 14, 15, 16, 17, 18, 19, 20]. However, until now, beyond the use of diamond nanocrystals as fluorescence markers [9, 10, 11, 12, 13], nothing was known about the quantum behaviour of a NV probe in the complex room temperature extra-cellular environment. For the first time we explore in detail the quantum dynamics of a NV probe in proximity to the ion channel, lipid bilayer and surrounding aqueous environment. Our theoretical results indicate that real-time detection of ion channel operation at millisecond resolution is possible by directly monitoring the quantum decoherence of the NV probe. With the potential to scan and scale-up to an array-based system this conclusion may have wide ranging implications for nanoscale biology and drug discovery.

The cell membrane is a critical regulator of life. Its importance is reflected by the fact that the majority of drugs target membrane interactions [5]. Ion channels allow for passive and selective diffusion of ions across the cell membrane [21], while ion pumps actively create and maintain the potential gradients across the membranes of living cells [22]. To monitor the effect of new drugs and drug delivery mechanisms a wide field ion channel monitoring capability is essential. However, there are significant challenges facing existing techniques stemming from the fact that membrane proteins, hosted in a lipid bilayer, require a complex environment to preserve their structural and functional integrity. Patch clamp techniques are generally invasive, quantitatively inaccurate, and difficult to scale up [23, 24, 25], while black lipid membranes [26, 27] often suffer from stability issues and can only host a limited number of membrane proteins.

Instead of altering the way ion channels and the lipid membrane are presented or even assembled for detection,

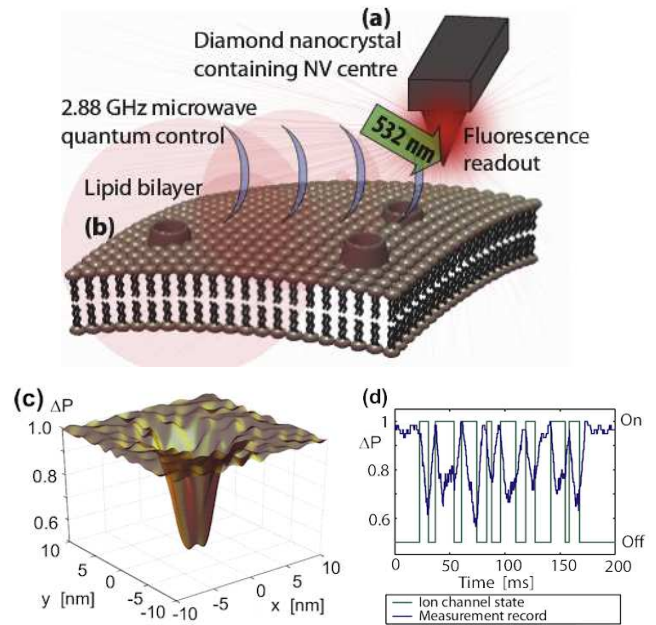


FIG. 1: Quantum decoherence imaging of ion channel operation. (a) A single nitrogen-vacancy (NV) defect in a diamond nanocrystal is placed on an AFM tip. The unique properties of the NV atomic level scheme allows for optically induced readout and microwave control of magnetic (spin) sub-levels. (b) The nearby cell membrane is host to channels permitting the flow of ions across the surface. The ion motion results in an effective fluctuating magnetic field at the NV position which decoheres the quantum state of the NV system. (c) This decoherence results in a decrease in fluorescence, which is most pronounced in regions close to the ion channel opening. (d) Changes in fluorescence also permit the temporal tracking of ion channel dynamics.

our approach is to consider a novel and inherently non-invasive in-situ detection method based on the quantum decoherence of a single-atom probe [18]. In this context, decoherence refers to the loss of quantum coherence between magnetic sub-levels of a controlled atom system due to interactions with an environment. Such superpositions of quantum states are generally fleeting in nature due to interactions with the environment, and the degree and timescale over which such quantum coherence is lost can be measured precisely. The immediate consequence of the fragility of the quantum coherence phenomenon is

that detecting the loss of quantum coherence (decoherence) in a single atom probe offers a unique monitor of biological function at the nanoscale.

The NV probe [Fig. 1] consists of a nano-crystal of diamond containing a nitrogen-vacancy (NV) defect placed at the end of an AFM tip, as recently demonstrated [8]. For biological applications a quantum probe must be submersible to be brought within nanometers of the sample structure, hence the NV system locked and protected in the ultra-stable diamond matrix [Fig. 1 (a)] is the system of choice. Of all the atomic systems known, the NV centre in diamond alone offers the controllable, robust and persistent quantum properties such room temperature nano-sensing applications will demand [9, 10, 28], as well as zero toxicity in a biological environment [13, 28, 29]. Theoretical proposals for the use of diamond nanocrystals containing a NV system as sensitive nanoscale magnetometers [14, 15, 16] have been followed closely by demonstrations in recent proof-of-principle experiments [8, 17, 19]. However, such nanoscale magnetometers employ only a fraction of the potential of the quantum resource at hand and do not have the sensitivity to detect the minute magnetic moment fluctuations associated with ion channel operation. In contrast, our results show that measuring the quantum decoherence of the NV induced by the ion flux provides a highly sensitive monitoring capability for the ion channel problem, well beyond the limits of magnetometer time-averaged field sensitivity [20].

In order to determine the sensitivity of the NV probe to the ion channel signal we describe, for the first time, the lipid membrane, embedded ion channels, and the immediate surroundings as a fluctuating electromagnetic environment and quantitatively assess each effect on the quantum coherence of the NV centre. We consider the net magnetic field due to diffusion of nuclei, atoms and molecules in the immediate surroundings of the nanocrystal containing the NV system and the extent to which each source will decohere the quantum state of the NV. We find that, over and above these background sources, the decoherence of the NV spin levels is in fact highly sensitive to the particular signal due to the ion flux through a single ion channel. Our theoretical findings demonstrate the potential of this approach to revolutionize the way ion channels and potentially other membrane bound proteins or interacting species are characterized and measured, particularly when scale-up and scanning capabilities are considered.

This paper is organized as follows. We begin by describing the quantum decoherence imaging system [Fig. 1] implemented using an NV centre in a realistic technology platform. The biological system is described in detail, considering the various sources of magnetic field fluctuations due to atomic and molecular processes in the membrane itself and in the surrounding media; and their effect on the decoherence of the optically monitored NV sys-

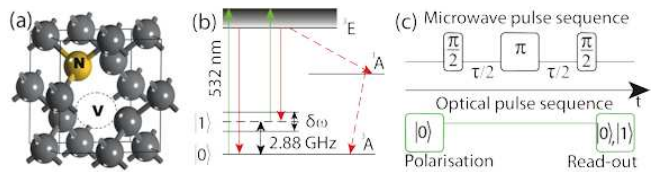


FIG. 2: (a) NV-centre diamond lattice defect. (b) NV spin detection through optical excitation and emission cycle. Magnetic sublevels $m_s = 0$ and $m_s = \pm 1$ are split by a $D=2.88$ GHz crystal field. Degeneracy between the $m_s = \pm 1$ sublevels is lifted by a Zeeman shift, $\delta\omega$. Application of 532 nm green light induces a spin-dependent photoluminescence and pumping into the $m_s = 0$ ground state. (c) Microwave and optical pulse sequences for coherent control and readout.

tem. Estimates of the sensitivity of the NV decoherence to various magnetic field fluctuation regimes (amplitude and frequency) are made which indicate the ability to detect ion channel switch-on/off events. Finally, we conduct large scale numerical simulations of the time evolution of the NV spin system including all magnetic field generating processes. This acts to verify the analytic picture, and provides quantitative results for the monitoring and scanning capabilities of the system.

The energy level scheme of the C_{3v} -symmetric NV system [Fig. 2(b)] consists of ground (3A), excited (3E) and meta-stable (1A) states. The ground state manifold has spin sub-levels ($m = 0, \pm 1$), which in zero field are split by 2.88 GHz. In a background magnetic field the lowest two states ($m = 0, +1$) are readily accessible by microwave control. An important property of the NV system is that under optical excitation the spin levels are readily distinguishable by a difference in fluorescence, hence spin-state readout is achieved by purely optical means [30, 31]. Because of this relative simplicity of control and readout, the quantum properties of the NV system, including the interaction with the immediate crystalline environment, have been well probed [32, 33]. Remarkably for the decoherence imaging application, the coherence time of the spin levels is very long even at room temperature: in type 1b nanocrystals $T_2 \sim 1\mu s$, and in isotopically engineered diamond can be as long as 1.8 ms[19] with the use of a spin-echo microwave control sequence [Fig. 2(c)].

Typical ion channel species K^+ , Ca^{2+} , Na^+ , and nearby water molecules are electron spin paired, so any magnetic signal due to ion channel operation will be primarily from the motion of nuclear spins. Ions and water molecules enter the channel in thermal equilibrium with random spin orientations, and move through the channel over a μs timescale. The monitoring of ion channel activity occurs via measurement of the contrast in probe behavior between the on and off states of the ion channel. This then requires the dephasing due to ion channel activity to be at least comparable to that due to the fluctuating background magnetic signal. We must therefore

account for the decoherence of the NV quantum state due to the diffusion of water molecules, buffer molecules, saline components as well as the transversal diffusion of lipid molecules in the cell membrane.

The n th nuclear spin with charge q_n , gyromagnetic ratio γ_n , velocity \vec{v}_n and spin vector \vec{S}_n , interacts with the NV spin vector \vec{P} and gyromagnetic ratio γ_p through the time-dependent dipole dominated interaction:

$$H_{\text{int}}(t) = \sum_{n=1}^N \kappa_{\text{dip}}^{(n)} \left[\frac{\vec{P} \cdot \vec{S}_n}{r_n^3(t)} - 3 \frac{\vec{P} \cdot \vec{r}_n(t) \vec{S}_n \cdot \vec{r}_n(t)}{r_n^5(t)} \right] \quad (1)$$

where $\kappa_{\text{dip}}^{(n)} \equiv \frac{\mu_0}{4\pi} \hbar^2 \gamma_p \gamma_n$ are the probe-ion coupling strengths, and $\vec{r}_n(t)$ is the time-dependent ion-probe separation. Additional Biot-Savart fields generated by the ion motion, both in the channel and the extracellular environment, are several orders of magnitude smaller than this dipole interaction and are neglected here. Any macroscopic fields due to intracellular ion currents are of nano-Tesla (nT) order and are effectively static over T_2 timescales. These effects will thus be suppressed by the spin-echo pulse sequence.

In Fig. 3(a) we show typical field traces at a probe height of 1-10nm above the ion channel, generated by the ambient environment and the on-set of ion-flow as the channel opens. The contribution to the net field at the NV probe position from the various background diffusion processes dominate the ion channel signal in terms of their amplitude. Critically, since the magnetometer mode detects the field by acquiring phase over the coherence time of the NV centre, both the ion channel signal and background are well below the $\text{nT Hz}^{-1/2}$ sensitivity limit of the magnetometer over the (~ 1 ns) self-correlated timescales of the environment. However, the effect of the various sources on the decoherence rate of the NV centre are distinguishable because the amplitude-fluctuation frequency scales are very different, leading to remarkably different dephasing behaviour.

To understand this effect, we need to consider the full quantum evolution of the NV probe. In the midst of this environment the probe's quantum state, described by the density matrix $\rho(t)$, evolves according to the Liouville equation, $\frac{d}{dt}\rho(t) = -\frac{i}{\hbar} [H(t)\rho(t) - \rho(t)H(t)]$, where $\rho(t)$ is the incoherent thermal average over all possible unitary evolutions of the entire system, as described by the full Hamiltonian, $H = H_{\text{nv}} + H_{\text{int}} + H_{\text{bg}}$, where H_{nv} is the Hamiltonian of the NV system, and H_{int} describes the interaction of the NV system with the background environment (e.g. diffusion of ortho spin water species and ions in solution) and any intrinsic coupling to the local crystal environment (e.g. due to ^{13}C nuclei or interface effects). The evolution of the background system due to self interaction is described by H_{bg} , which, in the present methodology, is used to obtain the noise spectra of the various background processes. We note that the following analysis assumes dephasing to be the dominant

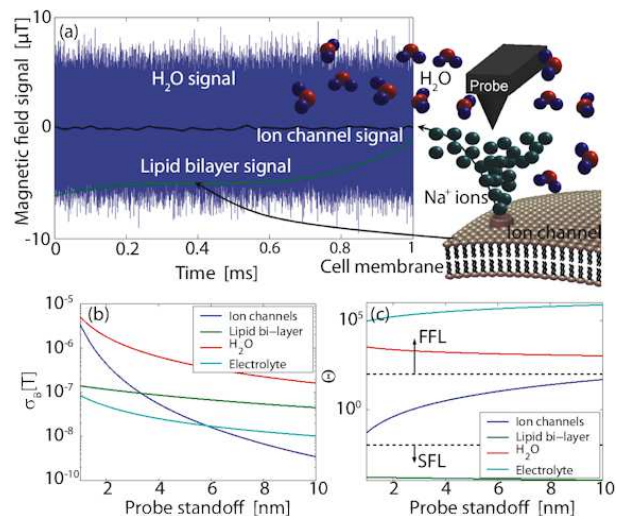


FIG. 3: (a) Typical magnetic field signals from water, ion channel and lipid bilayer sources at a probe standoff of 4 nm over a 1 ms timescale. (b) Comparison of σ_B for various sources of magnetic fields. (c) Fluctuation regime, $\Theta = f_e / \gamma_p \sigma_B$, for magnetic field sources vs probe standoff. Rapidly fluctuating fields ($\Theta \gg 1$) are said to be in the fast-fluctuating limit (FFL). Slowly fluctuating fields ($\Theta \ll 1$) are in the slow fluctuation limit (SFL). The ion channel signal exists in the $\Theta \sim 1$ regime, and therefore has an optimal dephasing effect on the NV probe.

decoherence channel in the system. We ignore relaxation processes since all magnetic fields considered are at least 4 orders of magnitude less than the effective crystal field of $D/\gamma_p \sim 0.2$ T, and are hence unable to flip the probe spin over relevant timescales. Phonon excitation in the diamond crystal leads to relaxation times of the order of 100s [19] and may also be ignored. Before moving onto the numerical simulations we consider some important features of the problem.

The decoherence rate of the NV centre is governed by the accumulated phase variance during the control cycle. Maximal dephasing due to a fluctuating field will occur at the cross-over point between the fast (FFL) and slow (SFL) fluctuation regimes [20]. A measure of this cross-over point is the dimensionless ratio $\Theta \equiv f_e / \gamma_p \sigma_B$, where $\tau_e = 1/f_e$ is the correlation time of the fluctuating signal, with cross-over at $\Theta \sim 1$. We can estimate the field standard deviation σ_B^{ic} due to the random nuclear spin of ions and bound water molecules moving in an ion channel (ic) as:

$$\sigma_B^{\text{ic}} \sim \frac{\mu_0}{4\pi} \frac{1}{h_p^3} \sqrt{N_{\text{ion}} \mu_{\text{ion}}^2 + N_{\text{H}_2\text{O}} \mu_{\text{H}_2\text{O}}^2}. \quad (2)$$

The fluctuation strength of the ion channel magnetic field, σ_B^{ic} , is plotted in Fig. 3(b) as a function of the probe stand-off distance, h_p . Ion flux rates are of the order of $\sim 5 \times 10^{-4}$ ions $\text{ns}^{-1} \text{nm}^{-2}$ [34], giving an effective dipole field fluctuation rate of $f_e \sim 3 \times 10^4$ Hz. For probe-

channel separations of 2-8nm, values of Θ range from 0.4 to 40 [Fig. 3(c)]. Thus, the ion channel flow hovers near the cross-over point, with an induced dephasing rate of $\Gamma_{ic} \sim 10^4 - 10^5$ Hz.

We now consider the dephasing effects of the various sources of background magnetic fields. The first source of background noise is the fluctuating magnetic field arising from the motion of the water molecules and ions throughout the aqueous solution. Due to the nuclear spins of the hydrogen atoms, liquid water consists of a mixture of spin neutral (para) and spin-1 (ortho) molecules. The equilibrium ratio of ortho to para molecules (OP ratio) is 3:1 [35], making 75% of water molecules magnetically active. In biological conditions, dissolved ions occur in concentrations 2-3 orders of magnitude below this and are ignored here (they are important however for calculations of the induced Stark shift, see below). The RMS strength of the field due to the aqueous solution is

$$\sigma_B^{H_2O} \sim g_H \mu_N \frac{\mu_0}{2\pi} \sqrt{n_{H_2O} \frac{\pi}{h_p^3}}. \quad (3)$$

This magnetic field is therefore 1-2 orders of magnitude stronger than the field from the ion channel [Fig 3(a,b)]. The fluctuation rate of the aqueous environment is dependent on the self diffusion rate of the water molecules. Using $D_{H_2O} = 3 \times 10^{-9} \text{ m}^2 \text{ s}^{-1}$, the fluctuation rate is $f_e^{H_2O} \sim D_{H_2O} / (2h_p)^2$. This places the magnetic field due to the aqueous solution in the fast-fluctuation regime, with $\Theta_{H_2O} \sim 10^3 - 10^4$ [Fig. 3(b)], giving a comparatively slow dephasing rate of $\Gamma_{H_2O} \sim f_e^{H_2O} \Theta_{H_2O}^{-2} \sim 100$ Hz and corresponding dephasing envelope $\mathcal{D}_{H_2O} = e^{-\Gamma_{H_2O} t}$.

An additional source of background dephasing is the lipid molecules comprising the cell membrane. Assuming magnetic contributions from hydrogen nuclei in the lipid molecules, lateral diffusion in the cell membrane gives rise to a fluctuating B-field, with a characteristic frequency related to the diffusion rate. Atomic hydrogen densities in the membrane are $n_H \sim 3 \times 10^{28} \text{ m}^{-3}$. At room temperature, the populations of the spin states of hydrogen will be equal, thus the RMS field strength is given by

$$\sigma_B^L \sim g_H \mu_N \frac{\mu_0}{8\pi} \sqrt{n \frac{5\pi}{4h_p^3}}. \quad (4)$$

The strength of the fluctuating field due to the lipid bilayer is of the order of 10^{-7} T [Fig. 3(a)]. The Diffusion constant for lateral Brownian motion of lipid molecules in lipid bilayers is $D_L = 2 \times 10^{-15} \text{ m}^2 \text{ s}^{-1}$ [36], giving a fluctuation frequency of $f_e^L \sim 125$ Hz and $\Theta_L \sim 10^{-4}$ [Fig. 3(d)]. At this frequency, any quasi-static field effects will be predominantly suppressed by the spin-echo refocusing. The leading-order (gradient-channel) dephasing rate is given by [20],

$$\Gamma_L \sim \frac{1}{2\sqrt{2}\sqrt{2}} \Theta_L^{-1/2} f_e^L + \mathcal{O}\left(\Theta_L^{-1/3} f_e^L\right), \quad (5)$$

giving rise to dephasing rates of the order $\Gamma_L \sim 100$ Hz, with corresponding dephasing envelope $\mathcal{D}_L(t) = e^{-\Gamma_L t^4}$.

The electric fields associated with the dissolved ions also interact with the NV centre via the ground state Stark effect. The coefficient for the frequency shift as a function of the electric field applied along the dominant (z) axis is given by $R_{3D} = 3.5 \times 10^{-3} \text{ Hz m V}^{-1}$ [37]. Fluctuations in the electric field may be related to an effective magnetic field via $B_z^{\text{eff}} = R_{3D} E_z / \gamma_p$, which may be used in an analysis similar to that above. An analysis using Debye-Hückel theory [38] shows charge fluctuations of an ionic solutions in a spherical region Λ of radius R behave as

$$\langle Q_\Lambda^2 \rangle = D_E k_B T (1 + \kappa R) e^{-\kappa R} \left[R \cosh(\kappa R) - \frac{\sinh(\kappa R)}{\kappa} \right], \quad (6)$$

where D_E is the diffusion coefficient of the electrolyte, and κ is the inverse Debye length (l_D); $l_D = 1/\kappa = 1.3$ nm for biological conditions. Whilst this analysis applies to a region Λ embedded in an infinite bulk electrolyte system, simulation results discussed below show very good agreement when applied to the system considered here. Eq. 6 is used to obtain the electric field variance, $\sigma_E = \sqrt{\langle E^2 \rangle - \langle E \rangle^2} \sim 10^6 \text{ Vm}^{-1}$, as a function of h_p . Relaxation times for electric field fluctuations are $\tau_e^E = \epsilon \epsilon_0 \rho_E$ [39], where ρ_E is the resistivity of the electrolyte, giving $f_e^E \sim 1/\tau_e^E = 1.4 \times 10^9$ Hz under biological conditions. Given the relatively low strength [Fig. 3(a)] and short relaxation time of the effective Stark induced magnetic field fluctuations ($\Theta \sim 10^5$) [Fig. 3(b)], we expect the charge fluctuations associated with ions in solution to have little effect on the evolution of the probe.

We now turn to the problem of non-invasively resolving the location of a sodium ion channel in a lipid bilayer membrane. When the channel is closed, the dephasing is the result of the background activity, and is defined by $\mathcal{D}_{\text{off}} = \mathcal{D}_{H_2O} \mathcal{D}_L \mathcal{D}_E \mathcal{D}_{13C}$. When the channel is open, the dephasing envelope is defined by $\mathcal{D}_{\text{on}} = \mathcal{D}_{\text{off}} \mathcal{D}_{ic}$. Maximum contrast will be achieved by optimising the spin-echo interrogation time, τ , to ensure $\mathcal{D}_{\text{off}} - \mathcal{D}_{\text{on}}$ is maximal. Thus in the vicinity of an open channel at the point of optimal contrast, $\tau \approx T_2/2$, we expect an ensemble ground state population of $P_{\text{on}}(T_2/2) = \frac{1}{2} [1 + \mathcal{D}_{\text{on}}(T_2/2)] = 0.61$, and $P_{\text{off}}(T_2/2) = \frac{1}{2} [1 + \mathcal{D}_{\text{off}}(T_2/2)] = 0.93$ otherwise. By scanning over an open ion channel and monitoring the probe via repeated measurements of the spin state, we may build up a population ensemble for each lateral point in the sample. The signal to noise ratio improves with the dwell time at each point. Fig. 4 shows simulated scans of a sodium ion channel with corresponding image acquisition times of 4, 40 and 400s. It should be noted here that the spatial resolution available with this technique is beyond that achievable by magnetic field measurements alone, since for large Θ , $\Delta P \propto B^2 \propto h_p^{-6}$.

We may employ similar techniques to temporally re-

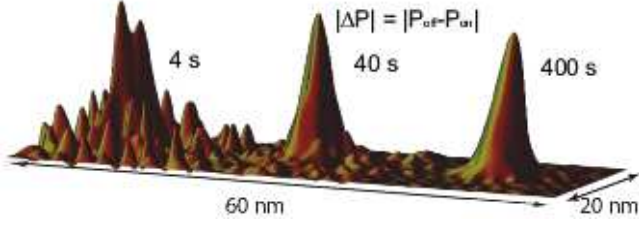


FIG. 4: Spatial information corresponding to the ion channel as a dephasing source. Relative population differences are plotted for pixel dwell times of 10, 100 and 1000 ms. Corresponding image acquisition times are 4, 40 and 400 s.

solve a sodium ion channel switch-on event. By monitoring a single point, we may build up a measurement record sequence, \mathcal{I} . In an experimental situation, the frequency with which measurements may be performed has an upper limit of $f_m = (\tau + \tau_m + \tau_{2\pi})^{-1}$, where $\tau_m \approx 900$ ns is the time required for photon collection, and $\tau_{2\pi}$ is the time required for all 3 microwave pulses. A potential trade-off exists between the increased dephasing due to longer interrogation times and the corresponding reduction in measurement frequency. Interrogation times are ultimately limited by the intrinsic T_2 time of the crystal. A second trade-off exists between the variance of a given set of N_τ consecutive measurements and the temporal resolution of the probe. For the monitoring of a switching event, the spin state population may be inferred with increased confidence by performing a running average over a larger number of data points, N_τ . However increasing N_τ will lead to a longer time lag before a definitive result is obtained. The uncertainty in the ion channel state goes as $\delta P \sim (\sqrt{N_\tau})^{-1}$, where N_τ is the number of points included in the dynamic averaging. We must take sufficient N_τ to ensure that $\delta P < \Delta P(\tau, h_p, T_2) = P_{\text{off}} - P_{\text{on}}$. The temporal resolution depends on the width of the dynamic average and is given by $\delta t \sim N_\tau(\tau + \tau_m)$, giving the relationship

$$\delta t = \frac{\tau + \tau_m}{\delta P^2} > \frac{\tau + \tau_m}{[\Delta P(\tau, h_p, T_2)]^2}. \quad (7)$$

We wish to minimise this function with respect to τ for a given stand-off (h_p) and crystal T_2 time.

In reality, not all crystals are manufactured with equal T_2 times. An important question is therefore, for a given T_2 , what is the best temporal resolution we may hope to achieve? Fig. 5(b) shows the optimal temporal resolution as a function of T_2 . It can be seen that δt improves monotonically with T_2 until T_2 exceeds the dephasing time due to the fluctuating background fields [Fig. 5(a)]. Beyond this point no advantage is found from extending T_2 .

A plot of δt as a function of τ is given in Fig. 5(c) for standoffs of 2-6 nm. Solid lines depict the resolution that maybe achieved with $T_2 = 300 \mu\text{s}$. Dashed lines represent the resolution that may be achieved by extending T_2 be-

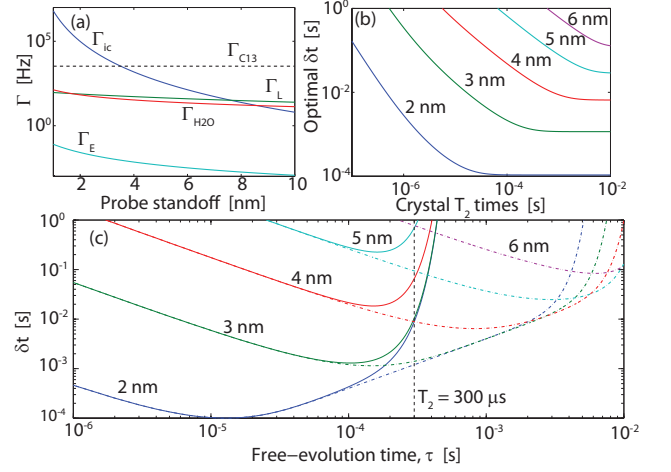


FIG. 5: (a) Dephasing rates due to the sources of magnetic field plotted as a function of probe standoff, h_p . (b) Optimum temporal resolution as a function of crystal T_2 times for $h_p = 2 - 6$ nm. (c) Temporal resolution as a function of interrogation time, τ , for separations of 2 - 6 nm and $T_2 = 300 \mu\text{s}$. Dashed lines show expected improvements from much longer T_2 times, $T_2 \gg \tau$.

yond the dephasing times of background fields. We see that δt diverges as $\tau \rightarrow T_2$, and is optimal for $\tau \rightarrow 1/\Gamma_{\text{ic}}$.

As an example of monitoring of ion channel behaviour, we consider a crystal with a T_2 time of $300 \mu\text{s}$ at a stand-off of 3 nm. Fig. 5(c) tells us that an optimal temporal resolution of $\delta t \sim 1.1$ ms may be achieved by choosing $\tau \sim 100 \mu\text{s}$. This in turn suggests an optimal running average will employ $N_\tau = \delta t (\tau + \tau_m)^{-1} \approx 11$ data points. Fig. 6(a) shows a simulated detection of a sodium ion channel switch-on event using $N_\tau = 20, 50$ and 100 points. The effect of increasing N_τ is shown to give poorer temporal resolution but also produces a lower variance in the signal. This may be necessary if there is little contrast between P_{off} and P_{on} . Conversely, decreasing N_τ results in an improvement to the temporal resolution but leads to a larger signal variation.

We now consider an ion channel switching between states after an average waiting time of 5 ms (200 Hz) [Fig. 6(b)]. To ensure the condition $\delta P < \Delta P$ is satisfied, we perform the analysis using $N_\tau = 20$, giving a resolution of $\delta t \approx 2$ ms. The blue curve shows the response of the NV population to changes in the ion channel state. Fourier transforms of the measurement record, $\mathcal{F}(\mathcal{I})$, are shown in Fig. 6(c)-(e). The switching dynamics are clearly resolvable for heights less than 6 nm. The dominant spectral frequency is 100 Hz which is half the 200 Hz switching rate as expected. Beyond 6 nm, the contrast between P_{off} and P_{on} is too small to be resolvable due to the T_2 limited temporal resolution, as given in Fig. 5(b). This may be improved via the manufacturing of nanocrystals with improved T_2 times, allowing for longer interrogation times [dashed curves, Fig. 5(c)].

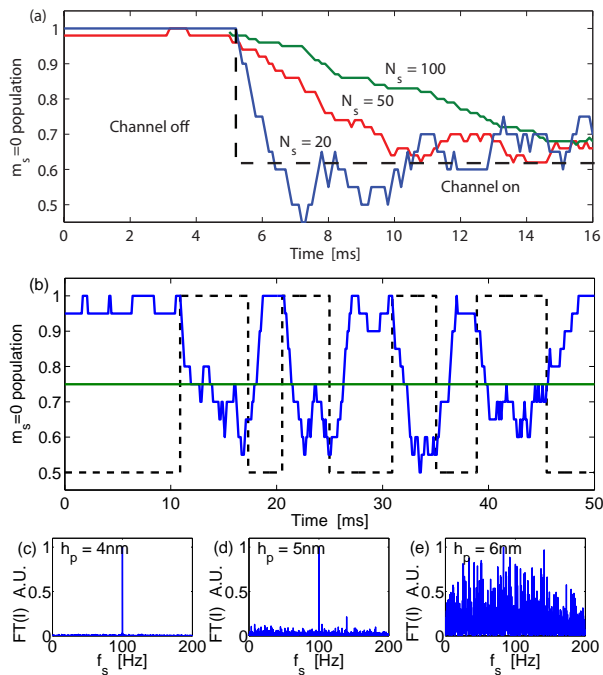


FIG. 6: (a) Plot illustrating the dependence of temporal resolution (δt) and signal variance (δP) on the number of data points included in the running average (N_s). (b) Simulated reconstruction of a sodium ion channel signal with a 200 Hz switching rate using optical readout of an NV centre (blue curve). The actual ion channel state (on/off) is depicted by the dashed line, and the green line depicts the analytic confidence threshold. Fourier transforms of measurement records are shown in (c)-(e) for stand-offs of 4, 5 and 6 nm respectively. Switching dynamics are clearly resolvable for $h_p < 6$ nm, beyond which there is little contrast between decoherence due to the ion channel signal and the background.

With regard to scale-up to a wide field imaging capability, beyond the obvious extrinsic scaling of the number of single channel detection elements (in conjunction with micro-confocal arrays), we consider an intrinsic scale-up strategy using many NV centres in a bulk diamond probe, with photons collected in a pixel arrangement. Since the activity of adjacent ion channels is correlated by the μm scale activity of the membrane, the fluorescence of adjacent NV centres will likewise be correlated, thus wide field detection will occur via a fluorescence contrast across the pixel. Implementation of this scheme involves a random distribution of NV centres in a bulk diamond crystal. The highest reported NV density is $2.8 \times 10^{24} \text{ m}^{-3}$ [40], giving typical NV-NV couplings of < 10 MHz which are strong enough to introduce significant additional decoherence. We seek a compromise between increased population contrast and increased decoherence rates due to higher NV densities, n_{nv} , given by $\Gamma_{\text{nv}} \sim \frac{\sqrt{2\pi}}{3} \frac{\hbar\mu_0}{4\pi} \gamma_p^2 n_{\text{nv}}$ [20].

For ion channel operation correlated across each pixel,

the total population contrast $\Delta\Phi$ between off and on states is obtained by averaging the local NV state population change $\Delta\Phi(\tau) = P_{\text{off}}(\vec{r}_i, \vec{r}_c, \tau) - P_{\text{on}}(\vec{r}_i, \vec{r}_c, \tau)$ over all NV positions \vec{r}_i and orientations; and ion channel positions \vec{r}_c and species; and maximizing with respect to τ . As an example, consider a crystal with $n_{\text{nv}} = 10^{24} \text{ m}^{-3}$ whose surface is brought within 3 nm of the cell membrane containing an sodium and potassium ion channel densities of $\sim 2 \times 10^{15} \text{ m}^{-2}$ [41]. Higher densities will yield better results, however these have not been realised experimentally as yet, and electron spins in residual nitrogen will begin to induce NV spin flips. We expect ion channel activity to be correlated across pixel areas of $1 \mu\text{m} \times 1 \mu\text{m}$, so the population contrast between off and on states is $\Delta\Phi \approx 15$. At these densities, the optimal interrogation time is $\tau \sim 0.8 \mu\text{s}$, yielding an improvement in the temporal resolution by a factor of 10,000, opening up the potential for single-shot measurements of ion channel activity across each pixel.

We have carried out an extensive analysis of the quantum dynamics of a NV diamond probe in the cell-membrane environment and determined the theoretical sensitivity for the detection, monitoring and imaging of single ion channel function through quantum decoherence. Using current demonstrated technology a temporal resolution in the 1-10 ms range is possible, with spatial resolution at the nanometer level. With the scope for scale-up and novel scanning modes, this fundamentally new detection mode has the potential to revolutionize the characterization of ion channel action, and possibly other membrane proteins, with important implications for molecular biology and drug discovery.

This work was supported by the Australian Research Council.

-
- [1] K. Lundstrom, Cell. Mol. Life Sci. **63**, 2597 (2006).
 - [2] B. Hille, *Ionic Channels of Excitable Membranes* (Sinauer Associates, Sunderland, MA, 2005), 3rd ed.
 - [3] Y. Fang, A. Frutos, and J. Lahiri, J. Am. Chem. Soc **124**, 2394 (2002).
 - [4] V. Yamazaki et al., BMC Biotechnol. **5**, 18 (2005).
 - [5] E. Reimhult and K. Kumar, Trends Biotechnol. **26**, 82 (2008).
 - [6] R. Jelinek and L. Silbert, Mol. Biosyst. **5**, 811 (2009).
 - [7] A. Demuro and I. Parker, J. Gen. Physiol. **126**, 179 (2005).
 - [8] G. Balasubramanian et al., Nature **455**, 648 (2008).
 - [9] F. Neugart et al., Nano Lett. **7**, 3588 (2007).
 - [10] C. C. Fu et al., Proc. Natl. Acad. Sci. U.S.A. **104**, 727 (2007).
 - [11] J. Chao et al., Biophys. J. **94**, 2199 (2007).
 - [12] O. Faklaris et al., Small **4**, 2236 (2008).
 - [13] A. Barnard, Analyst **134**, 1729 (2009).
 - [14] B. M. Chernobrod and G. P. Berman, J. Appl. Phys. **97**, 014903 (2004).
 - [15] C. L. Degen, Appl. Phys. Lett. **92**, 243111 (2008).

- [16] J. M. Taylor et al., *Nature Phys.* **4**, 810 (2008).
- [17] J. R. Maze et al., *Nature* **455**, 644 (2008).
- [18] J. H. Cole and L. C. L. Hollenberg, *Nanotech.* **20**, 495401 (2009).
- [19] G. Balasubramanian et al., *Nature Mat.* **8**, 383 (2009).
- [20] L. T. Hall et al., *Phys. Rev. Lett.*, In press (2009).
- [21] T. Ide et al., *Jpn. J. Physiol.* **52**, 429 (2002).
- [22] G. Baaken et al., *Lab Chip* **8**, 938 (2008).
- [23] S. Damjanovich, *Biophysical Aspects of Transmembrane Signalling* (Springer-Verlag, Berlin, Heidelberg, 2005), 1st ed.
- [24] E. Fenwick, A. Marty, and E. Neher, *J. Physiol* **331**, 599 (1982).
- [25] M. Quick, *Transmembrane Transporters* (John Wiley & Sons, Inc, Hoboken, NJ, 2002), 1st ed.
- [26] P. Mueller et al., *Nature* **194**, 979 (1962).
- [27] P. Mueller et al., *J. Phys. Chem.* **67**, 534 (1962).
- [28] S. Yu et al., *J. Am. Chem. Soc* **127**, 17604 (2005).
- [29] A. Schrand et al., *J. Phys. Chem. B. Lett.* **111**, 2 (2006).
- [30] F. Jelezko et al., *Appl. Phys. Lett.* **81**, 2160 (2002).
- [31] F. Jelezko and J. Wrachtrup, *Phys. Stat. Sol.* **203**, 3207 (2006).
- [32] F. Jelezko et al., *Phys. Rev. Lett.* **92**, 3207 (2004).
- [33] R. Hanson et al., *Science* **320**, 352 (2008).
- [34] H. Leontiadou et al., *Biophys. J.* **92**, 4209 (2007).
- [35] V. I. Tikhonov and A. A. Volkov, *Science* **296**, 2363 (2002).
- [36] H. Bannai et al., *Nature Protocols* **1**, 2628 (2006).
- [37] E. van Oort and M. Glasbeek, *Chem. Phys. Lett.* **168**, 529 (1990).
- [38] Y. C. Kim and M. E. Fisher, *Phys. Rev. E* **77**, 051502 (2008).
- [39] J. A. Fornes, *J. Colloid Interface Sci.* **222**, 97 (2000).
- [40] V. Acosta et al., *Phys. Rev. B* **80**, 115202 (2009).
- [41] P. Arhem and C. Blomberg, *Biosystems* **89**, 117 (2007).